

# A comprehensive experimental study of enhanced solid particle erosive resistance on the inner/outer surface of graphene nanoplatelets modified basalt/epoxy composite pipe

Harun Sepetcioglu<sup>1</sup>  | Seyit Mehmet Demet<sup>2</sup>  | Mehmet Bagci<sup>2</sup> 

<sup>1</sup>Department of Metallurgy and Materials Engineering, Faculty of Technology, Selçuk University, Konya, Türkiye

<sup>2</sup>Engineering and Natural Science Faculty, Mechanical Engineering Department, Konya Technical University, Konya, Türkiye

## Correspondence

Harun Sepetcioglu, Department of Metallurgy and Materials Engineering, Faculty of Technology, Selçuk University, Konya 42075, Türkiye.

Email: [harunsepet@selcuk.edu.tr](mailto:harunsepet@selcuk.edu.tr)

## Abstract

Basalt fiber reinforced polymer (BFRP) composite pipe is an excellent alternative to glass and carbon fiber reinforced composite pipes in industry and promising in high recycling for polymer composite used in aerospace, marine, and automotive. To enhance the solid particle erosion (SPE) properties of filament-wound BFRP composite pipe while preserving its mechanical properties, reinforced BFRP composite pipes were prepared to employ non-functionalized graphene nanoplatelets (GnPs) at a reinforcement concentration of 0.25 wt.% and ultrasonication mixing technique. The SPE behavior of GnPs reinforced and non-reinforced BFRP composite pipes were characterized by axial and radial positioning of the inner and outer surfaces of the pipes. In each case, the erosion rates of these composite pipes were evaluated at five impingement angles (30°, 45°, 60°, 75°, and 90°) and an impact velocity of 34 m/s. The erosion response of both BFRP composite pipes' outer surfaces showed a semi-ductile in the axial positioning, with a maximum erosion rate at a 60° impingement angle. However, these composite pipes' inner surfaces in the same positioning presented a maximum erosion rate at a 45° impingement angle. Besides, it is explored that the GnPs contribute to an improvement of approximately 10%–55% in erosive wear resistance of the non-reinforced BFRP composite pipes. The damage analysis of eroded surfaces was examined through scanning electron microscopy (SEM), and the GnPs effect upon composite pipes' erosion micro-mechanisms was presented and discussed in detail.

## Highlights

- GnPs increased the BFRP composite pipe's erosion resistance.
- Erosion rate on the inner surface increases due to particle accumulation.
- GnPs improved erosion behavior via solid lubrication and mechanical properties.

This is an open access article under the terms of the [Creative Commons Attribution-NonCommercial-NoDerivs](https://creativecommons.org/licenses/by-nc-nd/4.0/) License, which permits use and distribution in any medium, provided the original work is properly cited, the use is non-commercial and no modifications or adaptations are made.

© 2023 The Authors. *Polymer Composites* published by Wiley Periodicals LLC on behalf of Society of Plastics Engineers.

## KEYWORDS

BFR composite pipe, erosion resistance, erosive wear, graphene nanoplatelets, inner/outer surface

## 1 | INTRODUCTION

Recently, basalt fibers reinforced polymer (BFRP) composite pipes have been increasingly desirable for aerospace applications (rocket engine cases and launch tubes), marine (especially yacht poles), automotive, and so forth because of their lightweight, high modulus, strength, and comparatively low cost.<sup>1,2</sup> Understanding the erosion behavior of these pipes is crucial for ensuring their long-term structural integrity and reliable performance. In the last decade, Rafiee and co-workers have experimentally, theoretically, and numerically investigated the failure mechanisms and modes of composite pressure vessels,<sup>3</sup> pipes,<sup>4–6</sup> and cylinders<sup>7</sup> subjected to different loading conditions, including low-velocity impact and internal pressure. It is evident that considerable research efforts have been devoted to understanding the failure behavior of composite structures under various loading conditions. However, a comprehensive investigation focusing on filament-wound composite pipes' erosion behavior is currently lacking. During service life, the outer surface of the composite pipe may be subjected to wear by hard solid particles carried by strong winds in nature. On the other hand, their inner surface may be exposed to eroding in applications such as pipelines carrying sand slurries in petroleum refining or hydraulic transportation of solids.<sup>8,9</sup> However, these erosive environments that cause progressive material loss can result in wearing mechanically or chemically in engineering applications.<sup>10</sup>

In the literature, to the best of the author's knowledge, many researchers have investigated the mechanical<sup>11–13</sup> and tribological properties<sup>14–16</sup> of reinforced polymer composites (PCs). In general, they have reported high wear resistance<sup>17</sup> and low coefficient of friction of PCs<sup>18</sup> with the addition of various nanoparticles into the epoxy matrix. In the other works, the synergistic effect has been attributed to the improvements in superior wear properties obtained by adding two or more nano-reinforcements to the epoxy.<sup>19</sup> Furthermore, the research on the graphene nanoplatelets (GnPs) reinforced PCs of erosion behavior is remarkably limited. However, Prajapati et al. investigated the tribological properties of glass fabric-reinforced epoxy (GFRE) composite with 0.5–1 wt% of GnPs through a pin-on-disk wear testing tribometer. They reported that the frictional coefficient decreased with the addition of 0.5–1 wt% of GnPs, and increased the wear resistance of

the GFRE composites.<sup>20</sup> Moreover, it is reported that the GnPs improve the tribological performance of epoxy/basalt plates through their well-known solid lubricant properties and thermal conductivity.<sup>21–23</sup> Also, Berman et al. reported that graphene layers significantly reduced wear and coefficient of friction.<sup>24</sup>

There have been many studies of applications of reinforced PCs in solid particle erosion (SPE) works in the literature.<sup>25–29</sup> However, the SPE of reinforced composite pipes' inner and outer surfaces has not been inquired into the same extent as polymer-based plates. This lack of research reveals the challenge of the wear mechanism on the curved surface. The curvature radius of components has an important effect on erosion intensity. The greater the radius of curvature of the outer surface, the weaker its resistance to erosion.<sup>30</sup> When solid particles impinge on a curved surface, the direction of their impact changes due to the surface curvature. This change in impact angle alters the distribution of impact forces, leading to variations in erosion intensity across the curved surface. Additionally, the curvature influences the flow behavior of solid particles, causing changes in particle trajectories, velocities, and impact energies. Moreover, the magnitude of curvature on surface can affect the formation and development of erosion damage patterns. In this context, in the SPE tests performed in this study, the focus was not on the magnitude of the radius of curvature but instead on the pattern geometry occurring on the outer surface of the composite pipes. A filament-winding pattern on the composite pipe's outer surface appears because the BFRP pipes are produced via helical winding. This helical cycle of the fiber on the mandrel, the so-called mosaic, generates pattern geometry such as angle-ply laminate and zig-zag regions.<sup>31,32</sup> Consequently, the occurrence of these patterns can lead to several internal structure irregularities including wrinkle, undulation, resin starvation, delamination, porosity, void, fiber misalignment, fiber distortion, and fiber breakage.<sup>33–36</sup> All of these irregularities have the potential to impact the strength, integrity, and erosion resistance of the final composite structure. The total area of  $\pm 55$  zig-zag region is much smaller than the total area of  $\pm 55$  angle-ply laminate zones. Therefore, this study aims to investigate the SPE behavior of the inner and outer surfaces of GnPs modified BFRP composite pipes in the  $\pm 55$  angle-ply laminate regions, which are prone to erosion due to their filament-winding pattern. The outcomes of this study are

expected to contribute to the development of more durable and reliable composite pipes for various engineering applications.

## 2 | EXPERIMENTS

### 2.1 | Materials and production

The reinforced and unreinforced BFRP composite pipes were manufactured through the filament winding method shown in Figure 1, and it was preferred an EPIKOTE™ 828 LEVEL bisphenol and EPIKURE™ 866 hardener agent as epoxy resin system, monofilament 400 tex basalt as natural fiber with 13  $\mu\text{m}$ . For the epoxy modification, a non-functionalized GnPs with a surface area of 800  $\text{g}/\text{m}^2$ , a layer thickness of 3–7 nm, an average layer width of 1.5  $\mu\text{m}$ , and a purity of 99.9% were employed as nano reinforcement. The nano reinforcement, epoxy, and fiber were

provided by Nanografi, Hexion Inc, and Kamenny Vek Inc, respectively. Table 1 presents the properties of the epoxy system and basalt fiber.

To incorporate the GnPs into the polymer, the following steps were followed. First, the GnPs were arranged to achieve the desired weight ratio and then added to the neat epoxy resin. The mixture of GnPs and epoxy resin was subjected to mechanical mixing for a duration of 10–15 min. This step ensured the initial dispersion of GnPs throughout the epoxy matrix. Subsequently, the GnPs and epoxy resin mixture was subjected to ultrasonic mixing for 30 min to achieve a uniform dispersion of GnPs within the epoxy matrix. This process utilized high-frequency sound waves to enhance the homogeneity of the GnPs, ensuring their consistent distribution throughout the epoxy. After the ultrasonic mixing process, the mixture was maintained at a temperature of 60°C to facilitate the removal of air bubbles that may have formed during the mixing procedure. To further eliminate any

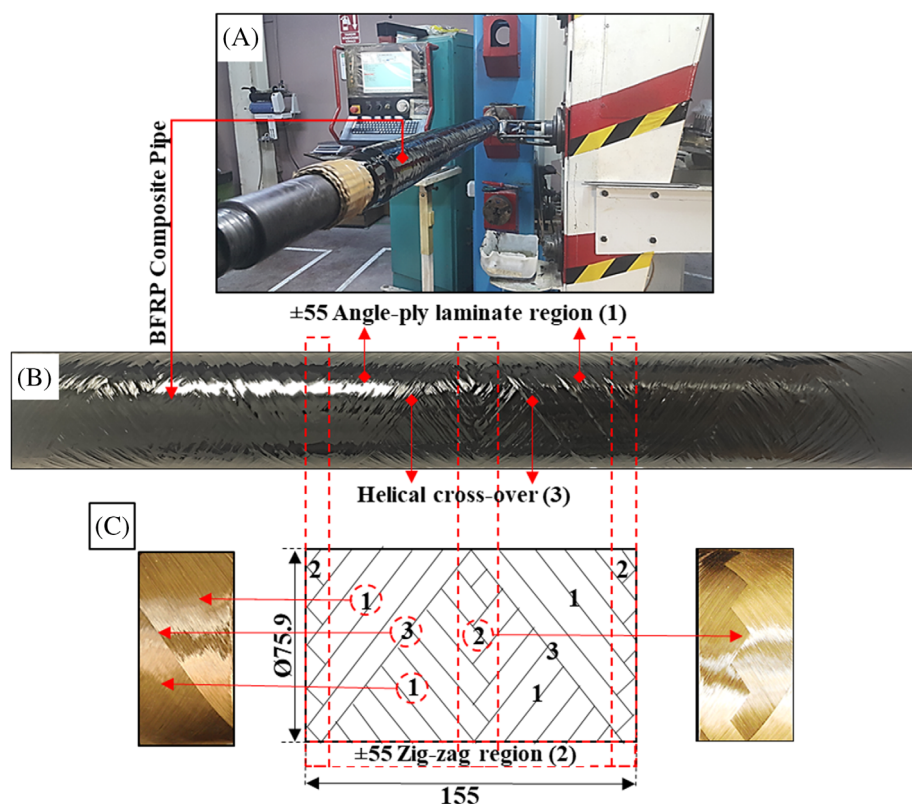


**FIGURE 1** Filament winding process (A), the BFRP composite pipe with mosaic pattern (B) winding pattern architecture in  $\pm 55$  angle-ply lamina and  $\pm 55$  zig-zag regions, and helical cross-over (C).

Type	Elasticity modulus E (GPa)	Ultimate tensile strength $\sigma$ (MPa)	Strain at the break $\epsilon$ (mm/mm)	Density $\rho$ ( $\text{g}/\text{cm}^3$ )
Basalt fiber	90–95	2900–3200	–	2.48
Epoxy resin	3.2	70–75	4–5	1.25

**TABLE 1** Properties of resin and fiber used in the production of BFRP composite pipe.

remaining air bubbles, a spoon was used to remove them from the surface of the mixture. Next, an anhydride-based hardener (EPIKURE™ 866) was added to the GnPs/epoxy mixture and mechanically mixed the mixture, resulting in the development of a cross-linked network. During the winding process, the basalt fibers were passed through a drum, allowing for the impregnation of the GnPs/epoxy mixture and ensuring comprehensive saturation of the basalt fibers with the GnPs/epoxy matrix. 0.25 wt.% GnPs reinforced BFRP composite pipe was considered in the current study because it was experimentally optimized to 0.25 wt.% in terms of mechanical properties in the previous works.<sup>1,2,37,38</sup>

## 2.2 | Erosion testing

The experimental equipment for the erosion rig is illustrated schematically in Figure 1A, and it complies with the ASTM G76-95 standard. The abrasive particles are accelerated by static pressure and delivered onto the specimen through a 10 mm diameter nozzle. The rotating disc method theoretically determines the velocity of the abrasive particles.<sup>39</sup> During the erosion test, the average velocity of the abrasive particle at 2 bar pressure was 34.0 m/s when the distance between the specimen and the nozzle was 10 mm. The inner and outer surfaces of reinforced and unreinforced BFRP composite pipes were subjected to an abrasive particle flow at a five impingement angle (30°, 45°, 60°, 75°, and 90°) and axial and

radial positioning, as shown in Figure 2B. The average erosion time was 24 s throughout the test, and the erosion wear in the composite pipes was determined by measuring the weight loss by employing a precision balance of  $\pm 0.0001$  g. The erosion test specimens of 50 mm length were cut from the composite pipe with a 1.0 m length, 75.9 mm outer diameter, and 1.95 mm wall thickness and mounted on a steel sample holder with 5 mm thick using plastic (Velcro) clamps. To carry out erosion tests on the internal surface of the pipes, surfaces perpendicular to the pipe's axis were cut at appropriate angles, as shown in Figure 2B; II, and IV. The erosion test parameters are summarized in Table 2.

TABLE 2 Erosion test conditions.

Test parameters	Description
Erodent	Aluminum oxide ( $\text{Al}_2\text{O}_3$ )
Erodent size	600 $\mu\text{m}$
Erodent shape	Angular
Hardness of erodent	Mohs 9
Density of $\text{Al}_2\text{O}_3$ particles	3.94 $\text{g}/\text{cm}^3$
Impingement angles	30–90°
Impact velocity	34 m/s
Specimen positioning	Axial and radial
Erodent feed rate	24 g/s
Test temperature	20–22°C
Nozzle to specimen distance	10 mm

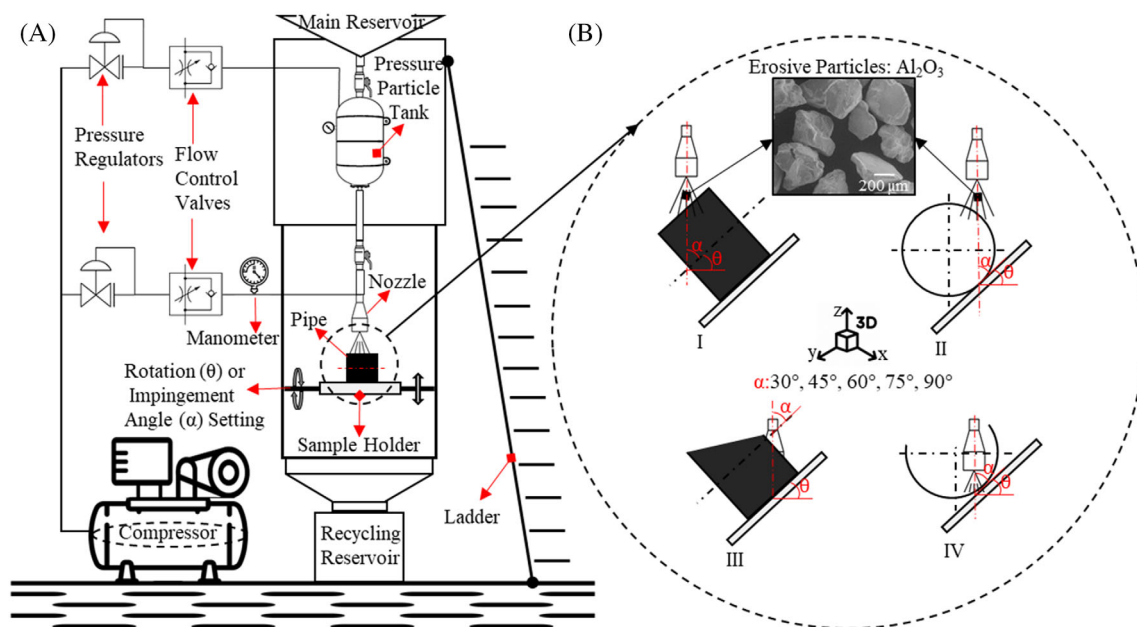


FIGURE 2 Schematic diagram of SPE rig (A), Definition of impingement angle, and BFRP composite pipe positionings (B); axial and radial positioning of the outer surface of the pipe (I and II), axial and radial positioning of the inner surface of the pipe (III and IV).

## 2.3 | Damage analysis of eroded region on the specimen

Erosion damages formed on the inner and outer surfaces of the composite pipes after the erosion test were cut for fractographic analysis, and then samples were coated with a 3–4 nm thick gold layer for scanning electron microscopy (SEM) analysis. Micro and macro damages containing the eroded surfaces' morphology and the material removal mechanism on the test specimens' inner and outer surfaces were detected utilizing a Zeiss LS10 SEM and a stereomicroscope.

## 3 | RESULTS AND DISCUSSION

### 3.1 | Erosion behavior

The contribution of GnPs with 0.25 wt.% on the erosion performance of BFRP composite pipe was quantitatively investigated utilizing the erosion rig, and the results were summarized in Tables 3 and 4. Figures 3 and 4 present the variation of the erosion rates as a function of impingement

angles ( $\alpha$ ) at different specimen positioning. Figure 3A shows that the erosion rate decreases with increasing impingement angle. However, the results in Figure 3B indicate that the erosion rate rises with increasing impingement angle up to 60° and then shows a decreasing trend again. According to these results, the response of all specimen's outer eroded surfaces was detected as ductile in the radial specimen positioning and semi-ductile in the axial specimen positioning.

The pipe's inner eroded surfaces' response is similar to the outer eroded surface behavior. Figure 4B shows that the erosion rate decreases with increasing impingement angle. In contrast, Figure 4A shows that the erosion rate increases with increasing impingement angle up to 45° and then decreases again. As mentioned above, it is seen that the inner surface of the pipe is ductile in radial positioning and semi-ductile in axial positioning. These results are consistent with studies<sup>40,41</sup> reporting that fiber-reinforced composites have ductile and semi-ductile erosion behavior.

The erosion rate of solid particles on a target surface can depend on the properties of the solid particle (such as size, shape, and hardness), the properties of the surface

**TABLE 3** Erosion rates of BFRP and GnPs/BFRP composite pipes' outer surfaces obtained in the positioning of axial and radial according to impingement angle.

Impingement angle (°)		Specimen positioning	Specimen types	Erosion rate (mg/kg)	Standard deviation	Improvement %
30	Outer surface	Axial	BFRP	211.75	±14.25	20.01
			GnPs/BFRP	169.28	±24.62	
	Radial	BFRP	87.5	±7.59	49.0	
		GnPs/BFRP	44.63	±1.09		
45	Axial	BFRP	203.50	±12.73	22.62	
		GnPs/BFRP	157.47	±25.08		
	Radial	BFRP	199.20	±20.88	45.56	
		GnPs/BFRP	108.46	±7.21		
	60	Axial	BFRP	153.23	±13.67	54.74
			GnPs/BFRP	69.35	±18.5	
Radial		BFRP	329.16	±25.92	45.46	
		GnPs/BFRP	179.50	±7.19		
75	Axial	BFRP	57.50	±5.24	35.86	
		GnPs/BFRP	36.88	±2.92		
	Radial	BFRP	65.53	±5.91	43.0	
		GnPs/BFRP	37.18	±1.5		
	90	Axial	BFRP	45.34	±10.19	19.32
			GnPs/BFRP	36.58	±1.71	
Radial		BFRP	45.17	±4.96	46.93	
		GnPs/BFRP	23.97	±0.89		

**TABLE 4** Erosion rates of BFRP and GnPs/BFRP composite pipes' inner surfaces obtained in the positioning of axial and radial according to impingement angle.

Impingement angle (°)	Specimen positioning	Specimen types	Erosion rate (mg/kg)	Standard deviation	Improvement %
30	Inner surface	BFRP	715.25	49.95	32.24
		GnPs/BFRP	484.59	5.88	
45	Axial	BFRP	877.72	41.58	23.98
		GnPs/BFRP	667.25	15.25	
	Radial	BFRP	792.75	37.56	29.14
		GnPs/BFRP	561.74	3.39	
60	Axial	BFRP	597.20	31.95	15.67
		GnPs/BFRP	503.58	13.65	
	Radial	BFRP	470.53	35.28	13.98
		GnPs/BFRP	404.75	2.75	
75	Axial	BFRP	368.52	45.22	16.0
		GnPs/BFRP	309.54	7.50	
	Radial	BFRP	290.12	37.54	28.0
		GnPs/BFRP	208.88	3.85	
90	Axial	BFRP	260.04	33.65	16.0
		GnPs/BFRP	218.43	4.75	
	Radial	BFRP	252.25	41.50	21.01
		GnPs/BFRP	199.25	0.75	
90	Radial	BFRP	252.24	45.60	10.86
		GnPs/BFRP	224.85	1.75	

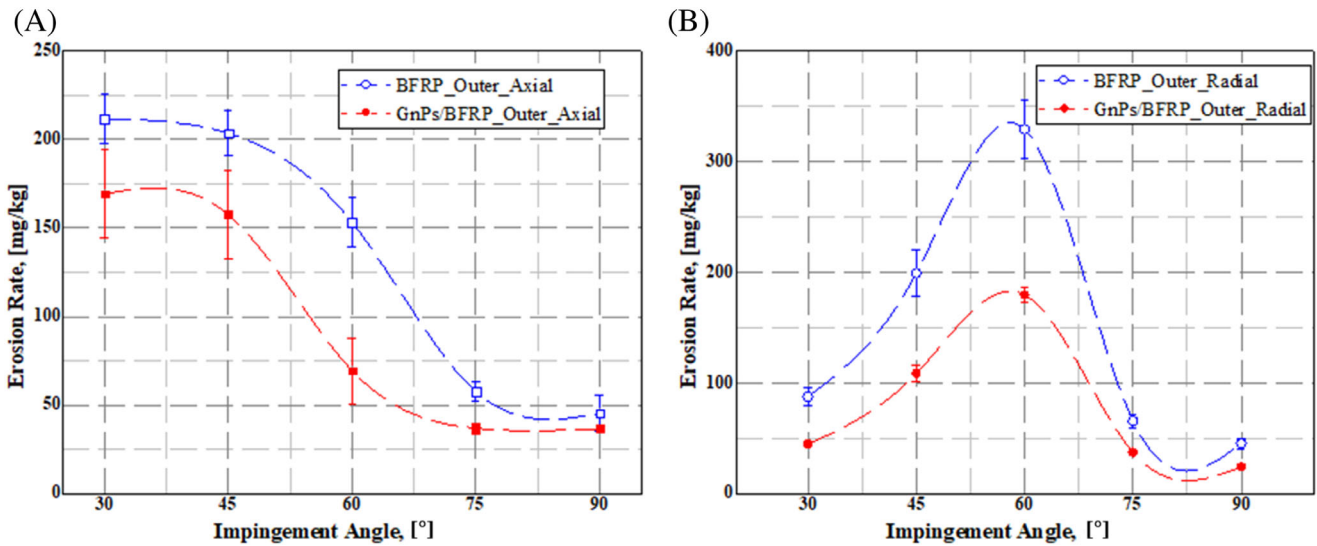


**FIGURE 3** The erosion rates of BFRP and GnPs/BFRP composite pipe as a function of an impingement angle at different positioning; (A) outer surface in the positioning of axial and (B) outer surface in the positioning of radial.

being eroded (such as surface roughness, surface energy, and material properties), and operating or test conditions (such as exposure time, particle concentration,

and impingement angle).<sup>14,15,39</sup> In the current study, we detected that a target object's surface having concave and convex also affects the erosion rate of solid particles. It was

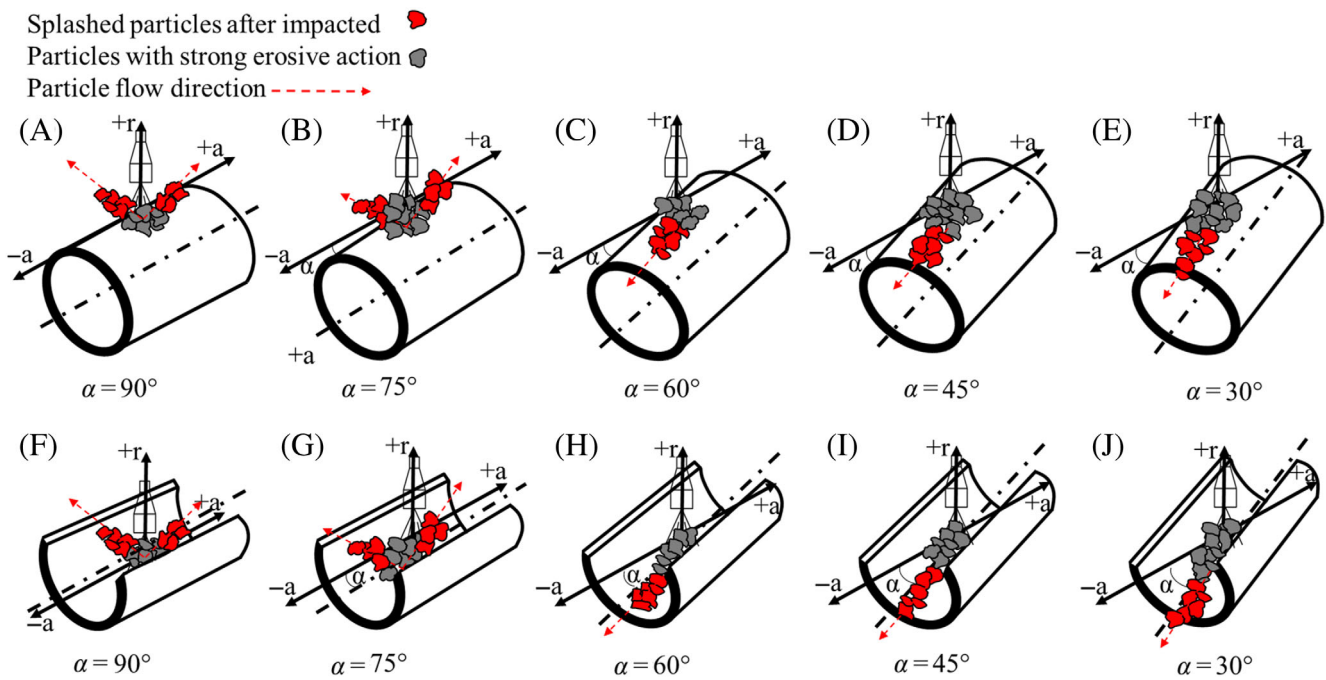


**FIGURE 4** Schematic views of the variation of the impingement angle in the BFR composite pipe inner (A–E) and inner (E–J) surfaces axial positioning. Illustrates the trajectory of splashed particles (in red) and particles that cause intense erosive action (in gray) as they flow in the direction of particle impact.

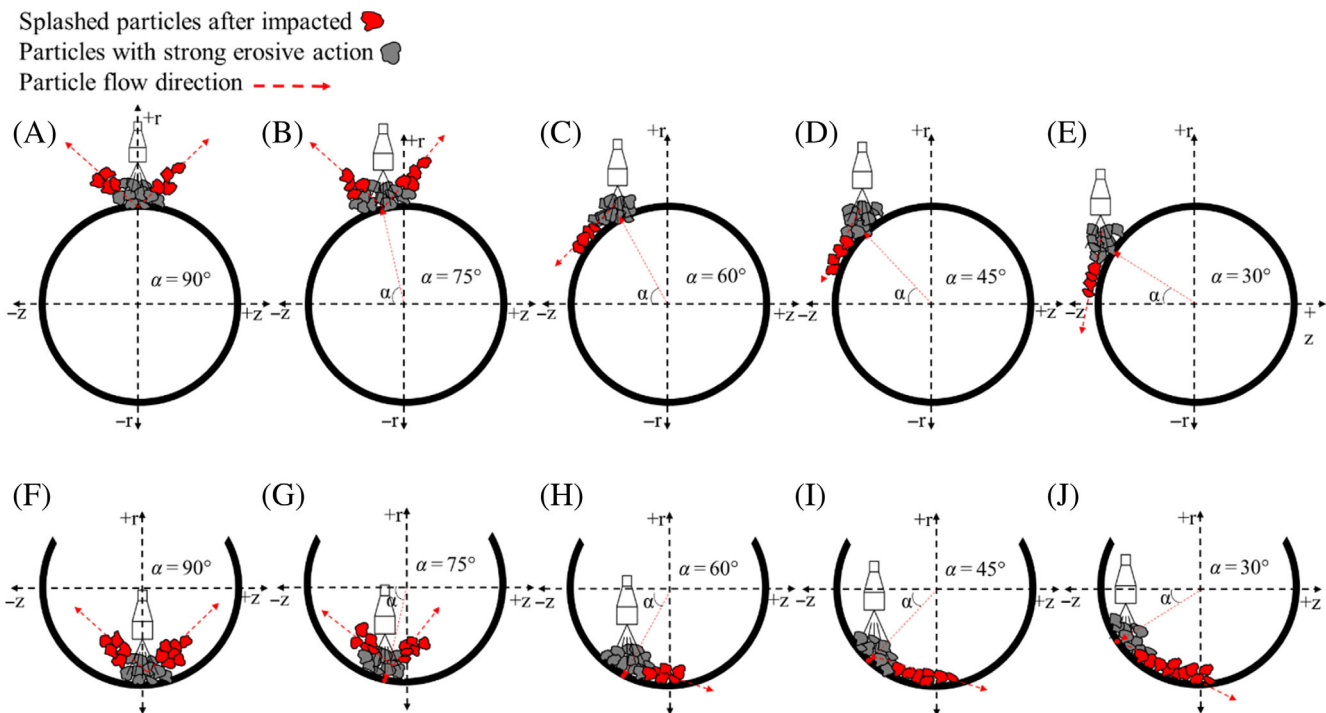


**FIGURE 5** Schematic views of the variation of the impingement angle in the BFR composite pipe outer (A–E) and inner (E–J) surfaces radial positioning. Illustrates the trajectory of splashed particles (in red) and particles that cause intense erosive action (in gray) as they flow in the direction of particle impact.

determined that the rate of SPE formed on the outer surface at all impact angles was lower than on the inner surface. The main reason is that a test specimen is an object

with a cylindrical geometry, as seen in Figures 4 and 5. For concave surfaces, the erosion rate is generally higher due to the focusing effect of the surface geometry. This

effect causes the particles to converge on the surface and create high-stress zones, which increase the erosion rate. In contrast, convex characters tend to have lower erosion rates due to the dispersal effect of the surface geometry. This effect causes the particles to disperse and reduce the concentration of high-stress zones, decreasing the erosion rate.

Figures 4A–E and 5A–E demonstrate that solid particles striking the outer surface have varying impact intensities, with some particles hitting the surface tangentially, resulting in less abrasive effects. This phenomenon is particularly prominent at impact angles of 45° and 30° when in radial positioning. In contrast to tests with axial positioning, a higher wear rate is observed at a 60° impact angle in radial positioning, resulting in semi-ductile erosive wear behavior on the outer surface due to the occurrence of cracks and material loss. In axial positioning on the outer surface, the impact angle has an active role in wear, as the force acting on the fiber and matrix increases with the cosine component of the impact angle. The erosion rate increases on the inner surface due to the concave geometric shape and cumulative impact of abrasive particles that accumulate on the surface, causing more wear. In axial positioning tests, the SPE rate in the internal surface reaches its maximum value at a 45° impact angle, resulting in semi-ductile erosion wear behavior. The maximum SPE rate is observed at a 60° impact angle on the outer surface in radial positioning, with abrasive particles causing cracks on the surface and resulting in significant material loss. The maximum material loss at a 45° impact angle on the inner surface is due to an increase in the particle/contact surface resulting from the solid particle focusing effect on the concave surface of the pipe, causing more material loss.

The erosion behavior of the GnPs reinforced BFRP composite pipes under various influences of impingement angle ( $\alpha$ ) was investigated. As seen in Figures 3 and 6, the erosion rate of all GnPs/BFRP composite pipes, as compared BFRPs, showed the same decreasing trend, regardless of axial and radial specimen positioning. In each impingement angle case, adding GnPs significantly reduces the erosion rate of the BFRP composite pipe. The minimum erosion rate is detected for the GnPs reinforced BFRP composite pipes at 90° of impingement angle in the radial specimen positioning of the outer surface. The maximum erosion rate values are 877.12 and 667.25 mg/kg for the BFRP and GnPs reinforced BFRP composite pipes at 90° of impingement angle in the radial specimen positioning of the outer surface, respectively. With the addition of 0.25 wt.% GnPs to the epoxy, it is reached a significant improvement of 54.74% in the erosion rate at 60° in the axial specimen positioning of the outer surface. The decrease in the erosion rate can be

attributed to the solid lubricating effect of GnPs<sup>42</sup> and the hardness and impact toughness increased by GnPs.<sup>1,38,43</sup> Another crucial effect of the GnPs is that it increases the strength on fiber/matrix interfacial.<sup>2,38,44</sup> The erosion response resulting from the high strength, extremely chemically inert trend, and the capability of being easily sheared of GnPs solid lubricants is considered to significantly enhance the SPE potential of BFRPs composite pipe.<sup>42</sup> The presence of GnPs in the epoxy matrix reduces the frictional forces between the erosive particles and the pipe surface, leading to a reduction in the erosion rate.<sup>21,45</sup> The GnPs-reinforced BFRP composite pipes exhibit superior resistance to SPE while providing highly elastic and impact properties compared to BFRP composite pipes.<sup>2,38</sup> The resistance of the pipes reinforced with GnPs against incoming abrasive particles rises due to the increased impact strength of epoxy reinforced with GnPs.<sup>1,37,38</sup> In addition, Sepetcioglu et al. informed that GnPs increased the hardness values of the BFRP composite pipe of GnPs reinforced.<sup>46</sup> The increased hardness value of BFRP composite pipe supports the reduction of SPE rate. GnPs improve the strength of the fiber/matrix interfacial because GnPs have high strength and stiffness, which can help to transfer stresses from the matrix to the fibers more effectively, and have a large surface area, which allows them to form strong chemical bonds with the matrix.<sup>2,45</sup> Kumar et al. discussed the impact of incorporating GnPs on the interlaminar shear strength (ILSS) of glass fiber-reinforced epoxy composites. They reported indicating an apparent increase in ILSS with the addition of GnPs.<sup>45</sup> The matrix dominates the ILSS properties of composites, so incorporating GnPs leads to better interfacial adhesion between the epoxy matrix and fibers and more effective stress transfer between them.<sup>47</sup> During an erosive particle impacts the surface of a BFRP composite, it causes damage by creating a scratch or a crack. Therefore, the interfacial bond and ILSS properties enhanced by GnPs resist this damage and prevent it from propagating further into the composite plies.

As reported in our previous study,<sup>39</sup> as the impingement angle decreases, the flow of particles on the pipe surface undergoes a transformation due to the angular position between the specimen and the nozzle. Consequently, the area of damage on the pipe's surface also changes. At an impingement angle of 60°, the influence of the cosine component becomes more pronounced compared to angles of 75° and 90°. At 45° and 30°, the particles contact a larger region on the pipe's surface. The plowing effect of the cosine component of erosive particles leads to significant damage on the outer surface of the pipe, resulting in a higher erosion rate characterized by greater material loss. As can be seen in Tables 3 and 4, the observation that the improvement efficiency of



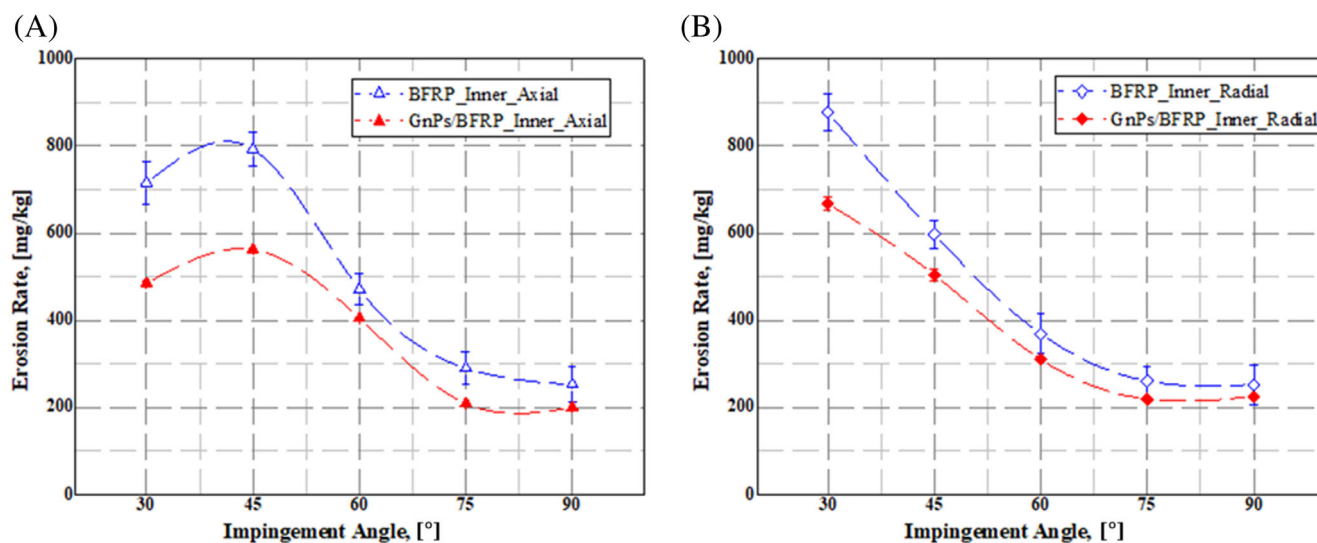


FIGURE 6 The erosion rates of BFRP and GnPs/BFRP composite pipe as a function of an impingement angle at different positioning; (A) inner surface in the positioning of axial and (B) inner surface in the positioning of radial.

GnPs in the erosion resistance decreases with a high erosion rate and increases with a low erosion rate on the inner and outer surfaces of GnPs/BFRP composite pipe can be attributed to several factors. The strong fiber/matrix interface can effectively inhibit the gap increase created by erosion and maintain the material's structural integrity. However, in a high erosion rate, the impacting particles have higher energy, leading to deeper penetration and larger damage to the pipe surface. This could result in reduced effectiveness of the GnPs in improving erosion-induced damage. High erosion rates can result in the formation of localized stress concentrations on the pipe surfaces due to the impact of solid particles. These stress concentrations can lead to crack initiation and propagation, which may not be effectively mitigated by the GnPs. The stress concentrations in a low erosion rate might be less severe, allowing the GnPs to distribute the stresses and reduce crack formation. It is important to note that the reasons mentioned above are hypothetical explanations based on experimental data and observation. The actual underlying mechanisms and interactions can vary depending on the composite production, test conditions, and experimental parameters used in the erosion test.

### 3.2 | Erosion mechanism

The SPE-induced damage images of BFRP and GnPs/BFRP composites pipes formed in  $\pm 55$  angle-ply lamina region is given in Figures 7–10. These SEM and stereomicroscope images were selected based on the maximum SPE rates on the outer and inner surfaces of neat BFRP

composite pipes. In order to characterize the shift from global to localized SPE phenomena, an approach was taken whereby SEM and stereomicroscopic images were merged to provide a comprehensive view of surface deformation. This enabled a comparative analysis of fiber and matrix damage penetration.

When a solid particle impacts a cylindrical object, the depth and extent of the damages may depend on several factors, such as the velocity, angle of impact, material properties (elasticity and strength) of the particle and the cylindrical object, and the concave and convex surfaces of the cylindrical object. Upon comparison of the stereo microscope images depicted in Figures 7 and 8A as well as Figures 9 and 10A, it is evident that the depth of the damage on the inner surfaces of the pipe and the regional width penetration is comparatively greater. The impact force generated by the impact of the solid particle on the outer (convex) surface was distributed along the surface, causing the pipe to deform slightly. On the other hand, it can be concluded that on the pipe's inner surface, the impact's force is concentrated in a smaller erosion area of concave origin, causing intense deformation.

The effects of GnPs on the damage of the outer and inner surfaces of BFRP composite pipes were investigated. The results are presented in Figures 7–10 for different impingement angles. For the outer surface, at a  $30^\circ$  impingement angle in axial positioning and a  $60^\circ$  impingement angle in radial positioning, adding GnPs reduced the depth of erosion damage but did not significantly affect the spread of regional damage on the pipe surface. Similarly, for the inner surface, at a  $45^\circ$  impingement angle in axial positioning and a  $30^\circ$  impingement angle in radial positioning, GnPs decreased the depth of

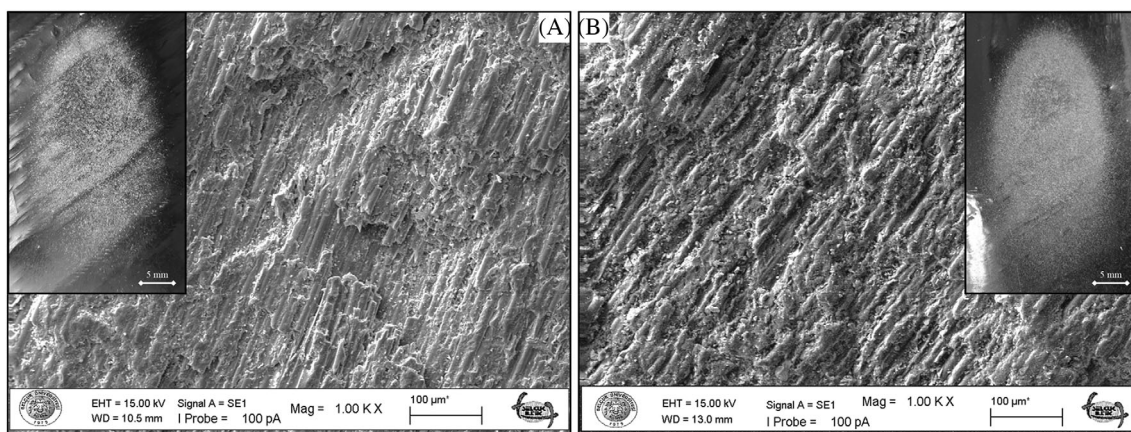


FIGURE 7 SEM images of matrix damages and fiber breakage on the outer surface at the 30° impingement angle in the positioning of axial: (A) BFRP and (B) GnPs/BFRP composite pipes.

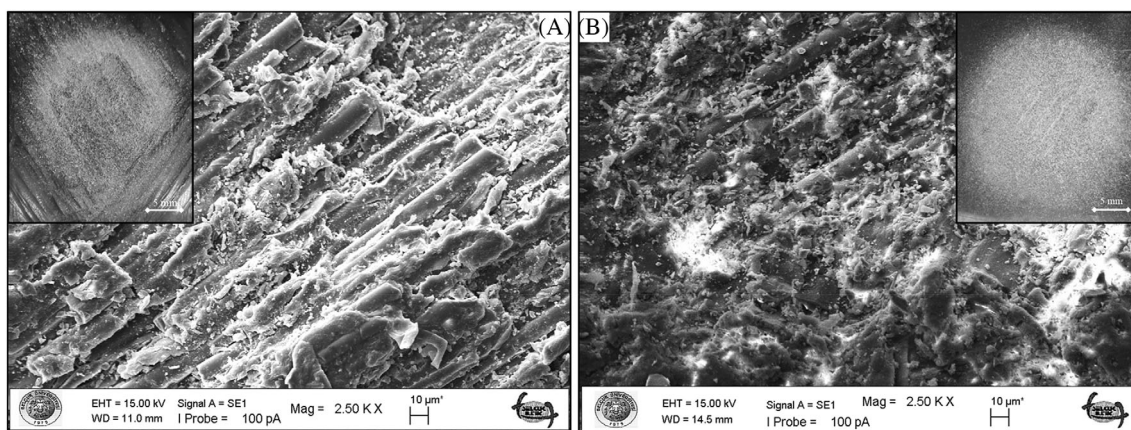


FIGURE 8 SEM images of matrix damages and fiber breakage on the outer surface at the 60° impingement angle in the positioning of radial: (A) BFRP and (B) GnPs/BFRP composite pipes.

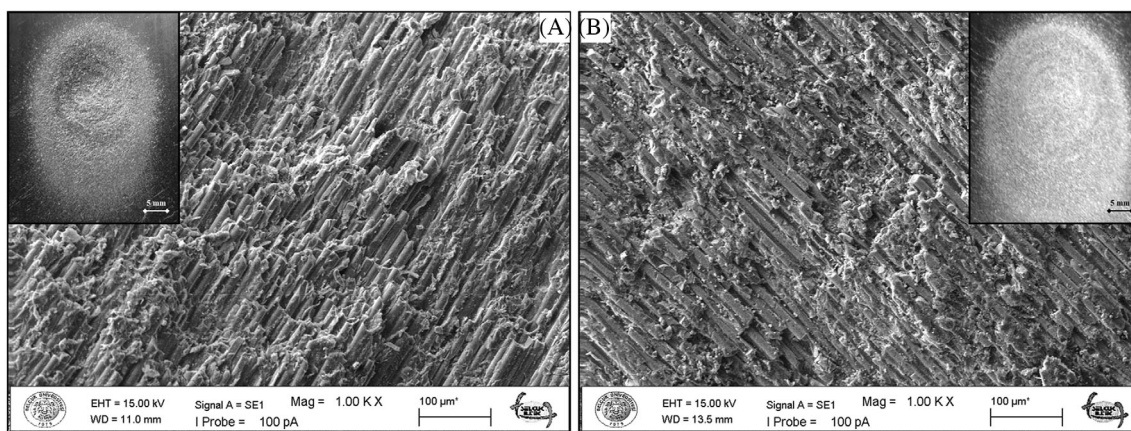
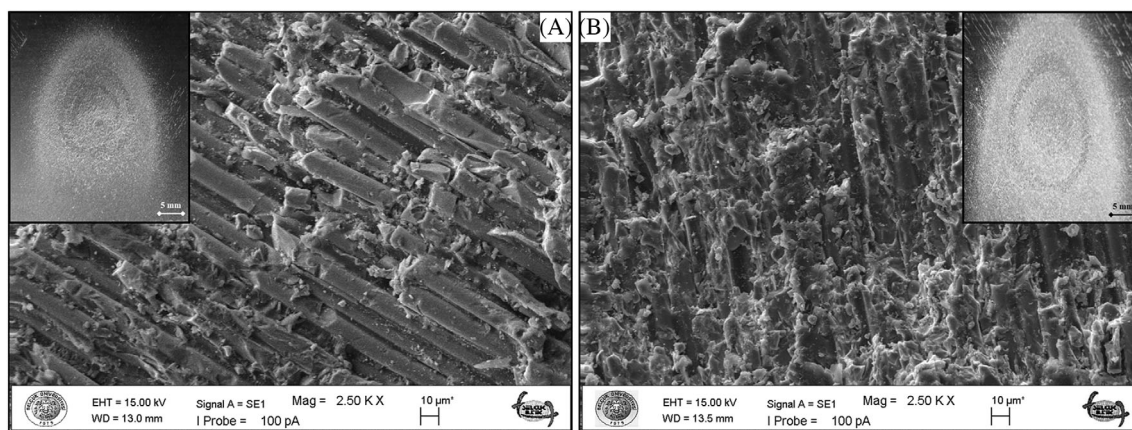


FIGURE 9 SEM images of matrix damages and fiber breakage on the inner surface at the 45° impingement angle in the positioning of axial: (A) BFRP and (B) GnPs/BFRP composite pipes.

erosion damage without affecting the spread of regional damage on the pipe surface. These findings suggest that GnPs can effectively reduce the depth of erosion damage

on both the inner and outer surfaces of BFRP composite pipes, but their impact on the regional damage area spread is limited.



**FIGURE 10** SEM images of matrix damages and fiber breakage on the inner surface at the 30° impingement angle in the positioning of radial: (A) BFRP and (B) GnPs/BFRP composite pipes.

SEM images revealed the presence of epoxy residues on the fibers in the damaged region formed in the inner and outer surfaces of the pipes. These residues' formation was attributed to the interfacial strength enrichment between the fiber and epoxy. The addition of GnPs significantly improved the adhesion of the epoxy to the fibers. Furthermore, SEM images of pipes doped with GnPs showed a much lower erosion depth than those without additives, indicating improved wear resistance. This improvement in erosion resistance is also contributed by the solid lubricating effect of GnPs, which reduces friction and erosion between the abrasive particle and the GnPs reinforced epoxy. In addition to improved erosion resistance, the addition of GnPs also led to an increase in the impact toughness of the epoxy. The increased impact toughness significantly supported the reduction of the SPE ratio with less fragmentation on the eroded surface. Increased interfacial strength resulted in an increase in the hardness value of the pipe. Overall, these results obtained from damaged surfaces suggest that the addition of GnPs can significantly enhance the mechanical properties of BFRP composite pipes, making them more durable and resistant to erosion.

## 4 | CONCLUSIONS


The SPE behavior of BFRP composite pipes was investigated, and it was found that the SPE rate of the inner surface was more due to the concave effect. However, by adding with GnPs, the depth of erosion was significantly reduced. The SEM images revealed that the epoxy residue on the fibers was due to the enrichment of the interfacial strength between the fiber and epoxy. GnPs were found to improve the interfacial strength, increase the impact toughness of the epoxy, enhance the hardness value of the pipe, and have a solid lubricant effect, resulting in a

decrease in erosion rate due to the improved erosion resistance. In conclusion, this study's results demonstrate that GnPs/BFRP composite pipes could be functional in various industrial applications, including oil and gas, water supply and sewage systems, chemical processing plants, and so on. These pipes' enhanced durability and toughness could play a role in increased efficiency, decreased maintenance costs, and improved safety. Further research could be conducted to investigate the feasibility of using GnPs/BFRP composite pipes in real-world scenarios and to optimize their performance for specific applications subjected to harsh erosion.

## DATA AVAILABILITY STATEMENT

The data that support the findings of this study are available from the corresponding author upon reasonable request.

## ORCID

Harun Sepetcioglu  <https://orcid.org/0000-0001-5746-4234>

Seyit Mehmet Demet  <https://orcid.org/0000-0002-9795-0939>

Mehmet Bagci  <https://orcid.org/0000-0001-6934-8660>

## REFERENCES

1. Sepetcioglu H. Experimental study on the effect of graphene nanoplatelets on the low-velocity impact response of pre-stressed filament wound basalt-based composite pressure vessels. *Polym Compos.* 2021;42:5527-5540.
2. Sepetcioglu H, Tarakcioglu N, Rafiee R. Experimental investigation of graphene nanoplatelets effect on the fatigue behavior of basalt/epoxy composite pressure vessels. *Thin-Walled Struct.* 2002;171:108672.
3. Rafiee R, Rashedi H, Rezaee S. Theoretical study of failure in composite pressure vessels subjected to low-velocity impact and internal pressure. *Front Struct Civ Eng.* 2020;14:1358.

4. Rafiee R. Experimental and theoretical investigations on the failure of filament wound GRP pipes. *Compos B: Eng.* 2013; 45:267.
5. Rafiee R, Amini A. Modeling and experimental evaluation of functional failure pressures in glass fiber reinforced polyester pipes. *Comput Mater Sci.* 2015;96:579-588.
6. Rafiee R, Reshadi F. Simulation of functional failure in GRP mortar pipes. *Compos Struct.* 2014;113:155-163.
7. Rafiee R, Ghorbanhosseini A, Rezaee S. Theoretical and numerical analyses of composite cylinders subjected to the low velocity impact. *Compos Struct.* 2019;226:111230.
8. Lin C-H, Zhu C. Relevance of particle transport in surface deposition and cleaning. *Developments in Surface Contamination and Cleaning.* Elsevier; 2008:267-297.
9. Friedrich K. Routes for achieving multifunctionality in reinforced polymers and composite structures. In: *Multifunctionality of Polymer Composites: Challenges and New Solutions.* Vol 3. Elsevier; 2015:41.
10. Patnaik A, Satapathy A, Chand N, Barkoula N, Biswas S. Solid particle erosion wear characteristics of fiber and particulate filled polymer composites: a review. *Wear.* 2010;268:249-263.
11. Murtaja Y, Lapčik L, Sepetcioglu H, et al. Enhancement of the mechanical properties of HDPE mineral nanocomposites by filler particles modulation of the matrix plastic/elastic behavior. *Nano Rev.* 2022;11:312-320.
12. Sepetcioglu H, Aydemir B. Short-term creep experiments and modeling on the effect of nano-sized calcium carbonate particles and applied stress on nonlinear viscoelastic behavior of high-density polyethylene. *J Polym Res.* 2022;29:1.
13. Sepetcioglu H. The effect of nanoclay on the nonlinear viscoelastic behavior of high-density polyethylene. *Polym Compos.* 2021;42:3468-3481.
14. Bagci M. Determination of solid particle erosion with Taguchi optimization approach of hybrid composite systems. *Tribol Int.* 2016;94:336-345.
15. Bagci M, Imrek H. Solid particle erosion behaviour of glass fibre reinforced boric acid filled epoxy resin composites. *Tribol Int.* 2011;44:1704-1710.
16. Imrek H, Demet S, Mech PI. Experimental investigation of wear behaviors of bronze and carbon-reinforced polytetrafluoroethylene alloy pivot pin bearings. *Eng J-J Eng.* 2014;228:1187-1194.
17. Wang Q-h, Zhang X-r, Pei X-q. Study on the friction and wear behavior of basalt fabric composites filled with graphite and nano-SiO<sub>2</sub>. *Mater des.* 2010;31:1403-1409.
18. Kim M, Rhee K, Lee B. Effect of carbon nanotube addition on the wear behavior of basalt/epoxy woven composites. *J Nanosci Nanotechnol.* 2013;13:5631-5635.
19. Mahesha C, Mohan N, Suprabha R. Three body abrasive wear studies on nanoclay/nano TiO<sub>2</sub> filled basalt-epoxy composites. *Mater Today: Proc.* 2017;4:3979-3986.
20. Prajapati PK, Kumar S, Singh K. Taguchi approach for comparative optimization of tribological behavior of glass fabric reinforced epoxy composite with and without graphene-nano platelets filler. *Mater Today: Proc.* 2023;72:1605-1612.
21. Kazemi-Khasragh E, Bahari-Sambran F, Siadati SMH, Eslami-Farsani R, Arbab Chirani S. The effects of surface-modified graphene nanoplatelets on the sliding wear properties of basalt fibers-reinforced epoxy composites. *J Appl Polym Sci.* 2019;136: 47986.
22. Kishore M, Amrita M, Kamesh B. Tribological properties of basalt-jute hybrid composite with graphene as nanofiller. *Mater Today: Proc.* 2021;43:244-249.
23. Zhou S, Wang J, Wang S, et al. Facile preparation of multiscale graphene-basalt fiber reinforcements and their enhanced mechanical and tribological properties for polyamide 6 composites. *Mater Chem Phys.* 2018;217:315-322.
24. Berman D, Erdemir A, Sumant AV. Few layer graphene to reduce wear and friction on sliding steel surfaces. *Carbon.* 2013;54:454.
25. Arani N, Rabba W, Papini M. Solid particle erosion of epoxy matrix composites reinforced by Al<sub>2</sub>O<sub>3</sub> spheres. *Tribol Int.* 2019;136:432-445.
26. Arjula S, Harsha A. Study of erosion efficiency of polymers and polymer composites. *Polym Test.* 2006;25:188-196.
27. Avcu E, Coban O, Özgür Bora M, Fidan S, Sinmazçelik T, Ersoy O. Possible use of volcanic ash as a filler in polyphenylene sulfide composites: thermal, mechanical, and erosive wear properties. *Polym Compos.* 2014;35:1826-1833.
28. Avcu E, Fidan S, Bora MÖ, Çoban O, Taşkıran İ, Sinmazçelik T. Solid particle erosive wear behavior of glass mat reinforced PPS composites: influence of erodent particle size, pressure, particle impingement angle, and velocity. *Adv Polym Technol.* 2013;32:386-E398.
29. Deo C, Acharya S. Solid particle erosion of lantana Camara fiber-reinforced polymer matrix composite. *Polym Plast Technol Eng.* 2009;48:1084-1087.
30. Zhou M, Liu H, Kang C, Wei X. Resistance of curved surfaces to the cavitation erosion produced through high-pressure submerged waterjet. *Wear.* 2019;440:203091.
31. Azeem M, Ya HH, Kumar M, et al. Application of filament winding technology in composite pressure vessels and challenges: a review. *J Energy Storage.* 2022;49:103468.
32. Rousseau J, Perreux D, Verdier N. The influence of winding patterns on the damage behaviour of filament-wound pipes. *Compos Sci Technol.* 1999;59:1439-1449.
33. Cohen D. Influence of filament winding parameters on composite vessel quality and strength. *Compos A: Appl Sci Manuf.* 1997;28:1035-1047.
34. McIlhagger A, Archer E, McIlhagger R. 3 - M anufacturing processes for composite materials and components for aerospace applications. In: Philip I, Constantinou S, eds. *Woodhead Publishing Series in Composites Science and Engineering, Polymer Composites in the Aerospace Industry.* 2nd ed. Woodhead Publishing; 2020:59-81.
35. Mertiny P, Ellyin F. Influence of the filament winding tension on physical and mechanical properties of reinforced composites. *Compos A: Appl Sci Manuf.* 2002;33:1615-1622.
36. Zindel D, Bakis CE. Nonlinear micromechanical model of filament-wound composites considering fiber undulation. *Mech Compos Mater.* 2011;47:73-94.
37. Sepetcioglu H, Tarakcioglu N. Fatigue behavior of graphene nanoplatelets reinforced and unreinforced basalt/epoxy composite pressure vessels subjected to low-velocity impact under internal pressure. *J Compos Mater.* 2021;55:4361-4373.
38. Sepetcioglu H, Tarakcioglu N. Effect of graphene Nanoplatelets on progressive failure behavior under internal pressure of composite cylindrical pressure vessels. *J Mater Eng Perform.* 2022; 31:2225-2239.

39. Demet SM, Sepetcioglu H, Bagci M. Solid particle erosion behavior on the outer surface of basalt/epoxy composite pipes produced by the filament winding technique. *Polymers*. 2023; 15:319.
40. Fouad Y, El-Meniawi M, Afifi A. Erosion behaviour of epoxy based unidirectional (GFRP) composite materials. *Alex Eng J*. 2011;50:29-34.
41. Rattan R, Bijwe J. Influence of impingement angle on solid particle erosion of carbon fabric reinforced polyetherimide composite. *Wear*. 2007;262:568-574.
42. Berman D, Erdemir A, Sumant AV. Graphene: a new emerging lubricant. *Mater Today*. 2014;17:31-42.
43. Rafiee MA, Rafiee J, Wang Z, Song H, Yu Z-Z. Enhanced mechanical properties of nanocomposites at low graphene content. *ACS Nano*. 2009;3:3884-3890.
44. Veerakumar VGS, Shanmugavel BP, Paskaramoorthy R, Harish S. The influence of graphene nanoplatelets on the tensile and impact behavior of glass-fiber-reinforced polymer composites. *J Mater Eng Perform*. 2021;30:596-609.
45. Kumar S, Singh KK, Ramkumar J. Comparative study of the influence of graphene nanoplatelets filler on the mechanical and tribological behavior of glass fabric-reinforced epoxy composites. *Polym Compos*. 2020;41:5403-5417.
46. Sepetcioglu H, Gunoz A, Kara M. Effect of hydrothermal ageing on the mechanical behaviour of graphene nanoplatelets reinforced basalt fibre epoxy composite pipes. *Polym Polym Compos*. 2021;29:166-S177.
47. Ahmadi-Moghadam B, Taheri F. Influence of graphene nanoplatelets on modes I, II and III interlaminar fracture toughness of fiber-reinforced polymer composites. *Eng Fract Mech*. 2015;143:97-107.

**How to cite this article:** Sepetcioglu H, Demet SM, Bagci M. A comprehensive experimental study of enhanced solid particle erosive resistance on the inner/outer surface of graphene nanoplatelets modified basalt/epoxy composite pipe. *Polym Compos*. 2023;44(10): 6944-6956. doi:[10.1002/pc.27609](https://doi.org/10.1002/pc.27609)